Fast-cure ionogel electrolytes with improved ion transport kinetics at room temperature

JANANI, Ronak, MADER, K <http://orcid.org/0000-0002-2524-6512>, ROBERTS, AJ, FARMILO, N <http://orcid.org/0000-0001-5311-590X> and SAMMON, C <http://orcid.org/0000-0003-1714-1726>

Published version

JANANI, Ronak, MADER, K, ROBERTS, AJ, FARMILO, N and SAMMON, C (2018). Fast-cure ionogel electrolytes with improved ion transport kinetics at room temperature. Journal of Power Sources, 406, 141-150.

Journal of Power Sources 406 (2018) 141–150

Fast-cure ionogel electrolytes with improved ion transport kinetics at room temperature

Ronak Janani[a], Kerstin Mader[a], Alexander John Roberts[b], Nicolas Farmilo[a], Chris Sammon[a],*

[a] Materials & Engineering Research Institute, Sheffield Hallam University, City Campus, Howard Street, Sheffield, S1 1WB, UK

[b] WMG, University of Warwick, Coventry, CV4 7AL, UK

Abstract

Fast-cure 1-ethyl-3-methylimidazolium trifluoromethanesulfonate based ionogels have been realised for the first time. The influence of curing temperature on the structure of ionogels and their performance as the electrolyte for electric double-layer capacitors (EDLCs) has been investigated. Hybrid ionogels were synthesised via a non-hydrolytic sol-gel route and were fully gelled post heat-treating at 125, 150, 175 and 200 °C for 60 min with minimal shrinkage. Charge-transfer resistance (a rate-limiting parameter in cell kinetics during charge/discharge cycles) was reduced by ~80% by increasing the heat-treatment temperature; this was partially attributed to the interlocking effect facilitated by high curing temperature. We report a maximum areal capacitance of 95 mF cm^{-2}. Due to ~40% increase in the penetrability coefficient of the ionic liquid, the electrode 'full' wetting time dropped from 48 to 5 h when the curing temperature was increased above 150 °C. These results were supported by SEM and Raman spectroscopy to characterise the effect of high temperature heat-treatment on the electrode-ionogel interface and the degree of electrode wetting by the ionic liquid. The fast-cure fabrication process for ionogels removes one of the major hurdles in their industrial application while the improved room temperature ion transport kinetics expands the potential application of ionic liquid-based electrochemical systems.

Keywords: Curing Temperature; Ionogel; Supercapacitor; Porous Electrode; Penetrability Coefficient, Electrode-Electrolyte Interface

Highlights:

- Room temperature kinetics of 4 heat-cured ionogels as EDLC electrolytes are studied
- Inter-particle ionic resistance is reduced by increasing curing temperature (T_c).
- Raman mapping proved greater ingress of IL within the electrode at higher T_c.
- Electrode wetting time was reduced to 5 hours at higher curing temperatures.

1. Introduction

Electric double layer capacitors (EDLCs) or supercapacitors are energy storage devices with higher energy density and power density compared to conventional capacitors and batteries respectively. Supercapacitors store energy by accumulating electrolyte charges within their porous electrodes and commercial EDLCs employ the use of propylene carbonates and acetonitrile electrolyte solvents [1–5]. The main drawback of these organic solvents is their flammable and volatile nature which raises safety concerns, but this can be addressed by using ionic liquid (IL) electrolytes [6,7]. Ionic liquids are salts with low melting point (typically below room temperature) that possess high thermal stability and excellent electrochemical characteristics, making them promising candidates to replace conventional electrolytes. In order to address the safety concern associated with electrolyte leakage, studies have been dedicated to the immobilisation of ionic liquids inside solid networks to create solid electrolytes which are often referred to as ionogels [8].

One-pot silica-based sol-gel synthesis at room temperature has been explored extensively as a facile fabrication route for ionogels. Numerous formulations have been suggested to design application-specific ionogels by optimising their mechanical strength and ionic conductivity [9,10]. Depending on the formulation and the fabrication environment, the process of gelation and drying of silica-based ionogels can typically take up to a few days to complete [10–12]. From an industrial perspective, where manufacturing speed is paramount by having a direct impact on the production costs, this is a major drawback.

Generally, the process of gelation consists of two major steps, namely hydrolysis and condensation. Acidic media catalyses the hydrolysis of

alkoxide groups (Si-OR) into hydroxyl groups (-OH) [9,13]. In addition, increasing the reaction temperature is an effective way to speed up condensation and drying stages, as elevated temperature promotes removal of volatiles and formation of covalent Si-O-Si bridges [14,15]. However, fast gelation and drying can introduce high capillary stress to the silica network and cause severe shrinkage and cracking. This can be resolved by incorporating (non-hydrolysable) organic functional groups into the structure to reduce the capillary stress and thus minimise shrinkage during gelation [15]. Fig. 1a represents the hypothesised final structure of a siloxane network where organic groups are present in the sol-gel backbone. To the best of our knowledge, the application of high curing temperatures (>100 °C) as a catalysing mechanism for ionogel synthesis and its influence on the resultant properties are currently unexplored. The physiochemical properties of ionic liquids are highly temperature dependant and thus, it is crucial to investigate the influence of curing temperature on the properties of ionogels as this can potentially minimise the gelation and drying time.

Conversely, operating-temperature dependency of the performance of energy storage devices containing ionic liquids has been widely studied. Zheng et al. investigated the electrochemical behaviour of a spinel $LiMn_2O_4$ electrode in trimethylhexylammonium (TMHA) bis(trifluoromethane) sulfonylimide (TFSI) ionic liquid electrolyte containing 1 M LiTFSI salt as a function of temperature [16]. They demonstrated that due to the high viscosity of the ionic liquid electrolyte the electrode-electrolyte interface resistance inside the electrochemical cell is strongly temperature dependant. In fact, they observed a ~90% drop in the interface resistance when the temperature was increased from 20 °C to 50 °C whilst conducting impedance measurements. Similarly, Rodrigues et al. reported a 50-fold decrease in the electrode-electrolyte interface resistance of a 2221o1-TFSI phosphoniumionic liquid-based lithium ion half cell when the temperature of the test environment was increased from 25 °C to 60 °C [17]. Negre et al. showed that the ionic conductivity of an ionogel containing a mixture of two bis(fluorosulfonyl)imide-based ionic liquids almost doubled to 11 mS cm^{-1} when temperature was raised from 20 to 80 °C [18]. However, the application of supercapacitors and batteries are not limited to high operating temperatures. The major challenge is to improve the performance of such systems at room temperature.

In this work, we attempt to address both the slow gelation and poor performance at room temperature by introducing heat during the process of ionogel condensation. The present work investigates the influence of curing temperature on the gelation time, penetrability coefficient of the ionic liquid, physical structure of ionogels and the room-temperature electrochemical performance of EDLC cells fabricated by sandwiching the heat-cured ionogels between activated carbon (AC) electrodes.

2. Experimental

2.1 Electrode preparation

Activated carbon electrodes were prepared by mixing YP50-F (Kuraray Chemical Co., Japan), 8 wt% polyvinylidene fluoride binder (PVdF, Solvay) in n-methyl pyrrolidinone (NMP, Fisher Scientific) and carbon black (Imerys) as a conductivity enhancer, in the ratio 87:8:5 in NMP, in a high torque mixer (Buhler, Switzerland) for less than 4 h. The mixed ink was then coated onto aluminium foil (current collector) using a reel to reel coater (Magtec, UK) with a three stage drier. The resultant electrode was further dried overnight under vacuum at 120 °C before light calendering. The electrodes utilised for this investigation were cut into 15 mm diameter disks with thickness of ~100 μm. The resultant mass loading of each electrode was ~5.38 mg cm^{-2}.

2.2 Electrolyte preparation

The ionogel electrolytes were synthesised using a simple non-hydrolytic sol-gel route. Firstly, 20 μL of tetramethylorthosilicate (TMOS, Sigma Aldrich, ≥98%) and 55 μL of methyltrimethoxysilane (MTMS, Sigma Aldrich, ≥98%) were mixed in a glass vial together with 200 μL of 1-ethyl-3-methylimidazolium trifluoromethanesulfonate ([Emim][TfO], Sigma Aldrich, ≥98%) under vigorous stirring (600 rpm) for 10 min using a magnetic stir bar. The process of hydrolysis was then initiated by adding 65 μL formic acid (FA, Aldrich ≥96%). This was followed by another 10 min mixing time. All of the chemicals were used as received. The TMOS: MTMS: FA: IL molar ratio was kept constant at 1: 3: 14: 8 for all samples.

2.3 EDLC fabrication

After the 20 min synthesis process described in 2.2, fixed volumes (60 μL) of the mixture were deposited onto activated carbon disks. The ionogel-coated electrodes were heated to four different temperatures (125, 150, 175 and 200 °C) using a ramp rate of 5 °C min^{-1} and held isothermally at the final temperature for 60 min. The total duration of heat-treatment ranged between 75 and 90 min. Once the heating process was completed, the ionogel coated AC electrodes were left to cool at room temperature for a minimum of 5 min. The double-layer supercapacitor cells were then sandwiched between CR2032 coin cells inside glove box under a nitrogen atmosphere to avoid any contamination.

2.4 Electrochemical characterisation

Electrochemical impedance spectroscopy (EIS) measurements of the EDLC cells were obtained using a PARSTAT 4000A potentiostat (Princeton Applied Research, USA). A 10 mV rms potential was applied oscillating around 0 V bias voltage over a frequency range of 100 kHz to 10 mHz. The cyclic voltammetry (CV) analysis was performed in a potential window of 2.5 V and at a scanning rate of 50 mV s^{-1}. The areal capacitance values were calculated based on the integration of enclosed area in the CV curves after 5 cycles. All electrochemical tests were taken periodically at room temperature across a time period of 48 h.

2.5 Contact angle measurements

Contact angle was measured on a OCA30 drop shape analyser (DataPhysics Instruments, Germany) using a polytetrafluoroethylene coated needle. The static contact angle between the activated carbon surface and a 2-μL ionic liquid drop was recorded at five different locations using SCA 20 software (version 3.50.1).

2.6 Viscosity measurements

The viscosity of the ionic liquid was measured using a MCR301 Rheometer (Anton Paar, UK) equipped with a bob and cup setup. A shear rate of 10 s^{-1} was utilized while the temperature was nominally raised from 25 to 200 °C at 2 °C min^{-1} ramping rate. These measurements were repeated 3 times and the mean value was reported. Due to limitations of the instrumentation, the actual maximum temperature achieved during measurements was 188 °C. Viscosity at 200 °C was therefore estimated by extrapolating the viscosity vs. temperature curve.

2.7 Surface tension measurements

Surface tension of [Emim][TfO] was measured using a DCAT25 tensiometer equipped with TEC250 temperature control chamber (DataPhysics Instruments GmbH, Germany). The chosen method for surface tension determination was the Wilhelmy plate method and therefore the standard platinum plate PT8 was used as the probe.

2.8 Scanning electron microscopy (SEM) characterisation

The morphology of the ionogel-coated electrodes was investigated using a Nova 200 NanoSEM (FEI, USA) at 10 kV.

2.9 Raman spectroscopy measurements

The spatial distribution of [Emim][TfO] at the cross section of the AC electrodes was characterised on an inVia Raman spectrometer equipped with an automated stage (Renishaw, UK) using 785 nm diode laser excitation. Spectra were collected between 200 and 3200 cm^{-1} utilising WiRE software (version 3.4). A line-map was acquired across the coated electrodes' cross section with a step size of 5 μm and a x5 objective which resulted in a degree of oversampling (spot size ~8 μm). The overall spatial distribution of each compound was extracted simultaneously from the Raman line-map using multivariate curve resolution (MCR, version 1.6) analysis software which is a useful tool in resolving multicomponent mixture systems using variety of algorithms. In the present study, the alternating least squares regression (ALS) algorithm was utilised to separate the data into i) spectra of different compounds present (referred to as number of factors) and ii) the relative intensity of each compound/factor at each location along the map.

3. Results and Discussion

By incorporating organic functional groups into the gel network, the capillary tension, shrinkage and cracking of ionogels caused by fast gelation can be reduced. Fig. 1a represents a hypothesised structure of a typical siloxane network where organic functional groups (represented by R) are located within the structure in a disordered manner. In the formulation utilised in this work, the hydrophobic methyl groups (derived from methyltrimethoxysilane) limit the formation of crosslinking Si-O-Si bridges in certain directions (i.e. where CH_3 groups are located) and hinder

the hydrolysis and condensation processes, counterbalancing the fast gelation tendency at high temperatures (to some extent). We rationalise that the presence of stable ≡Si-CH_3 groups in the silica monolith partially offsets the mechanical stress and thus the overall brittleness of the ionogels [19]. Fig. 1b displays the optical images of ionogel coated electrodes after being cured at 125, 150, 175 and 200 °C. As no flowing behaviour was observed upon tilting the electrode, all samples were considered to have been fully gelled after the heating process. As it is shown, no signs of cracking or shrinkage have been noted in the samples cured at the two lower temperatures. However, despite the presence of CH_3 groups in the gel matrix, a modest degree of shrinkage and cracking was observed in samples cured at 175 and 200 °C. In the case of the 200 °C curing temperature, rapid removal of volatiles has resulted in shrinkage and high capillary tension (greater than the incorporation of ≡Si-CH_3 could overcome) causing the formation of cracks. Small IL droplets can also be observed on the surface of ionogels (Fig. 1b). The population of these droplets reduces as the curing temperature is increased.

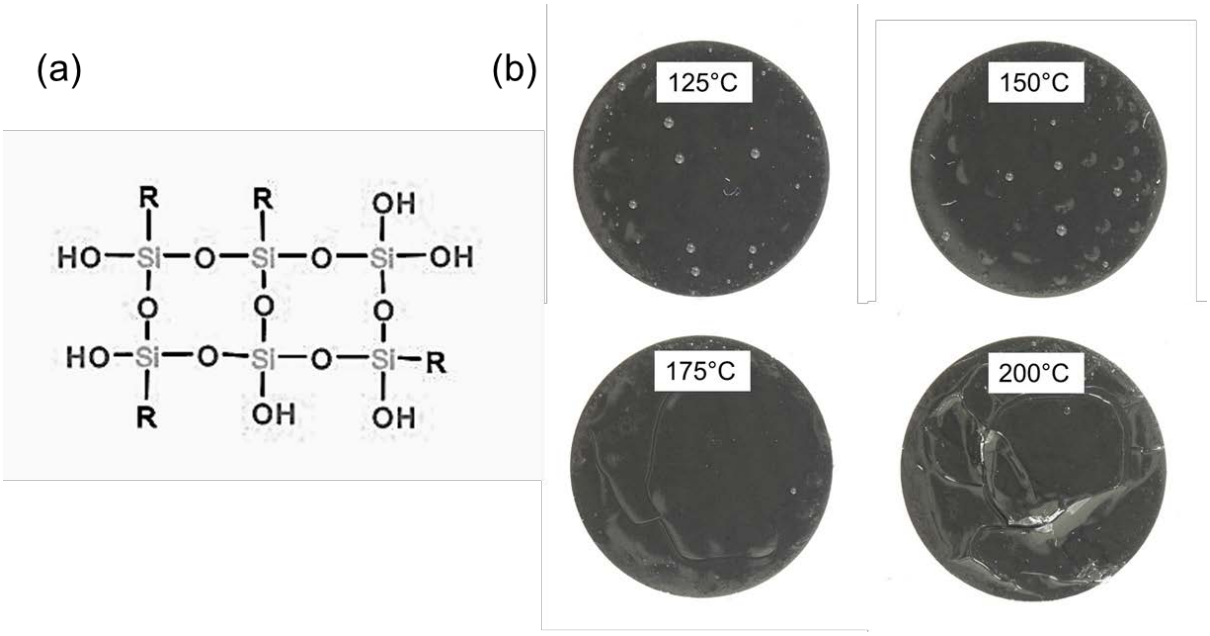

Fig. 1 (a) The hypothesised chemical structure of a typical siloxane group containing an organic functional group (R) and (b) the physical appearance of ionogel coated electrodes when cured at various temperatures ranging from 125 to 200°C.

3.1 Changes in penetrability coefficient of [Emim][TfO] with temperature

Ionic liquids are known for their relatively high viscosity at room temperature compared to other commercially used liquid electrolytes [17]. When heat is introduced to a system containing ILs, a considerable change in performance of the

system is to be expected. In the case of systems where IL is in contact with a porous structure, these variations are likely to translate into changes in the wetting rate of the porous network. Generally, the wetting rate of a porous electrode is dictated by the degree of spreading and penetration of the electrolyte [20]. The Lucas-Washburn equation (Eq. (1)) models the electrolyte movement in a porous electrode with the assumption of the porous network being an entity of capillaries:

$$k = \sqrt{\frac{r_{eff}\sigma \cos\theta}{2\eta}} \quad (1)$$

where k is the penetrability coefficient, r_{eff} is the effective radius of capillary, σ is the liquid-to-vapor surface tension, θ is the three phase contact angle and η is the viscosity. A higher k value is associated with faster liquid flow within the porous network. One must not forget that most of the porous electrodes are not an ensemble of evenly arranged capillaries but rather a complex network of pores oriented in random directions. Therefore, the focus in this study was not to evaluate the exact value of penetrability coefficient but to investigate the relative changes in k as a function of curing temperature. If one assumes that there are no changes in the effective pore size with temperature, the relative changes of k can be estimated using Eq. (2):

$$k \propto \sqrt{\frac{\sigma \cos\theta}{2\eta}} \quad (2)$$

Table 1 presents the measured surface tension and viscosity of [Emim][TfO] as a function of temperature, as well as the cosine of the three phase contact angle. The static contact angle between the activated carbon electrode and ionic liquid approaches 0° within 8 s at room temperature (~22 °C). Considering that surface tension is reduced with temperature, one can postulate that θ approaches 0° much faster at higher temperatures. For this reason, cosθ is assumed to be 1 in all cases from 22 to 200 °C. Thus changes in k become dependant on surface tension and viscosity assuming no change takes place in the effective pore radius. It was observed that, the viscosity of ionic liquid drops by ~55% when curing temperature is increased from 125 to 200 °C, while surface tension decreases by ~8%. This agrees with the literature [20,21] considering viscosity to be the main factor influencing

wetting rate. Based on these results, ~40% increase in the penetrability coefficient is expected when increasing the curing temperature from 125 to 200 °C.

Table 1 Influence of temperature on physical properties of [Emim][TfO].

Temperature / °C	σ / mN m^{-1}	$\cos\theta$	η / mPa s	$\sqrt{\frac{\sigma\cos\theta}{2\eta}}$ / (m s^{-1})$^{1/2}$
25°	40.51 ∓ 0.02	1	44.00 ∓ 0.21	0.68
125°	36.84 ∓ 0.04	1	4.90 ∓ 0.06	1.94
150°	35.94 ∓ 0.03	1	3.60 ∓ 0.10	2.23
175°	34.88 ∓ 0.06	1	2.70 ∓ 0.06	2.54
200°	33.84 ∓ 0.07	1	≅ 2.20	2.77

3.2 Effect of temperature on the physical structure of electrode-electrolyte interface

The SEM images of post-cure electrode cross sections are shown in Fig. 2. Starting from the left hand side within Fig. 2a, one can observe a thin layer of Al foil, upon which sits the porous activated carbon electrode and lastly, in direct contact with this, the dense ionogel solid electrolyte can be identified. The high porosity of the activated carbon electrodes explains their extensive application in energy storage systems as they provide large surface area and hence increase the maximum achievable capacity in such devices. As can be seen in Fig. 2a, the interface between the gel electrolyte and the AC electrode is sharp and clearly visible. This interface becomes more diffuse as the temperature is raised above 150 °C (Fig. 2b and d). At higher curing temperatures, ionogel is postulated to penetrate further through the electrode and mask the top surface of electrode as observed in the SEM images (Fig. 2c and d). In the latter cases, the electrode and the electrolyte are interpenetrated as a result of the heat-induced interlocking effect [22]. The porous structure of the AC electrodes cannot easily be discerned in samples treated at curing temperatures of 175 and 200 °C. In addition, a degree of delamination from the Al foil can be seen in all four samples. The reasons for delamination of the AC

electrode from the Al foil are i) defects caused during the process of cutting the electrodes and ii) the impact of heat on the binder. The PVdF binder in the AC electrodes has a melting point of 177 °C [23] and thus, it goes through a melting and re-solidification process when the curing temperature is 175 °C and above. The influence of this 'contact loss', melting and re-solidifying of PVdF is discussed in the following section (3.3).

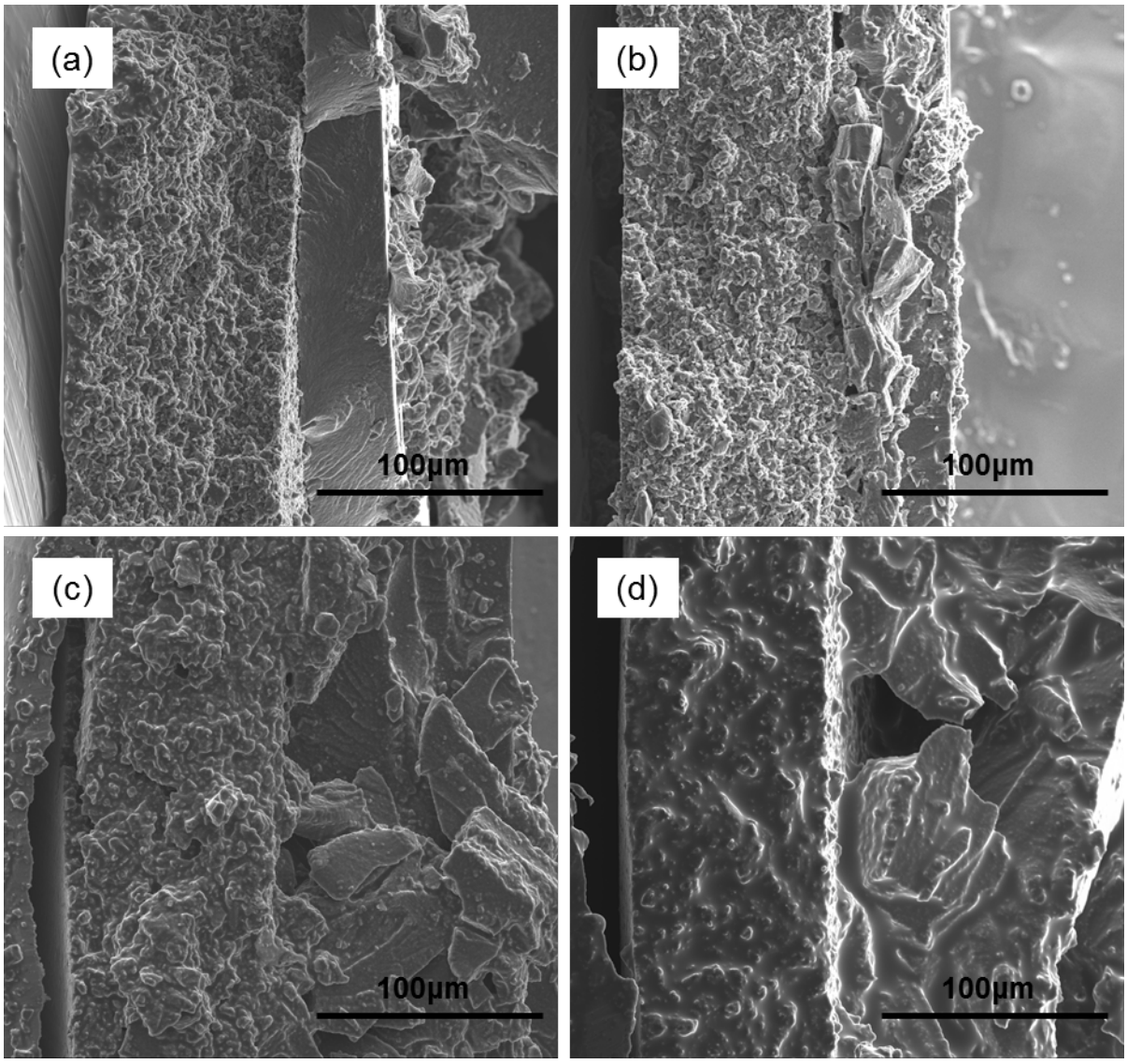

Fig. 2 (a) Electron microscope cross section images of ionogel-coated AC electrodes cured at: (a) 125°C, (b) 150°C, (c) 175°C and (d) 200°C. From left to right in each image, traces of Al foil, porous activated carbon electrode and ionogel electrolyte can be identified.

3.3 Evolution of impedance with temperature and time

A Nyquist plot, generated from EIS measurements, shows the impedance response of a system as a function of frequency. Fig. 3 displays the Nyquist plots of cells with

ionogel electrolytes cured at four different temperatures after 0, 5, 24 and 48 h of assembling the cell. A Nyquist plot is divided into 3 main regions of high, mid-range and low frequency which carry valuable information about the electrochemical system being investigated. The high frequency x-axis (real impedance, Z') intercept is referred to as intercept resistance (R_i). At this point in an EIS measurement, the frequency is too high for any mass transport to take place. Therefore, intercept resistance is a representation of the bulk electrolyte resistance [24,25] although in some cases this resistance has also been attributed to electrolyte-electrode-current collector contact resistance [26]. In the case of the ionogels this resistance mainly corresponds to the ionic resistance within the silica structure. This is followed by the mid-range frequency semi-circle which has been assigned to a number of ionic and electrical components inside an EDLC: (a) intrinsic resistance of the electrode [27] , (b) electrical contact resistance between current collector and the electrode active material [27,28], (c) inter-particle ionic impedance [27,29], (d) ion transport processes [25] and (e) electrolyte starvation (in the case of low electrolyte concentration) [30,31]. Therefore, the dominating component influencing the charge transfer resistance (R_{ct}, given by the diameter of the mid-range frequency semi-circle) is dependent on the system being investigated. Systems containing ionic liquids are expected to have dominating ionic resistances influencing the mid-frequency semi-circle due to high viscosity and relatively large size ions of ILs. However, the influence of electrical resistances should not be neglected. It is important to note that the nature of R_{ct} in EDLCs with porous electrodes [24,27] is different from that in psuedocapacitors which is mainly associated with the Faradaic processes taking place in the cell [32].

Finally, the Lower frequency region (straight line) in a Nyquist plot is assosiated with the intraparticle diffusion of electrolyte ions and double-layer formation (Z_{dl}) [25,26]. When the frequency becomes low enough, the overall impedance of the cell increases linearly at an angle with x-axis of 45° to 90°. A large inclining angle (i.e. sharp increase in imaginary impedance, Z'') represents facile ion diffusion [26]. Figure 4a breaks down the three different regions in a Nyquist plot.

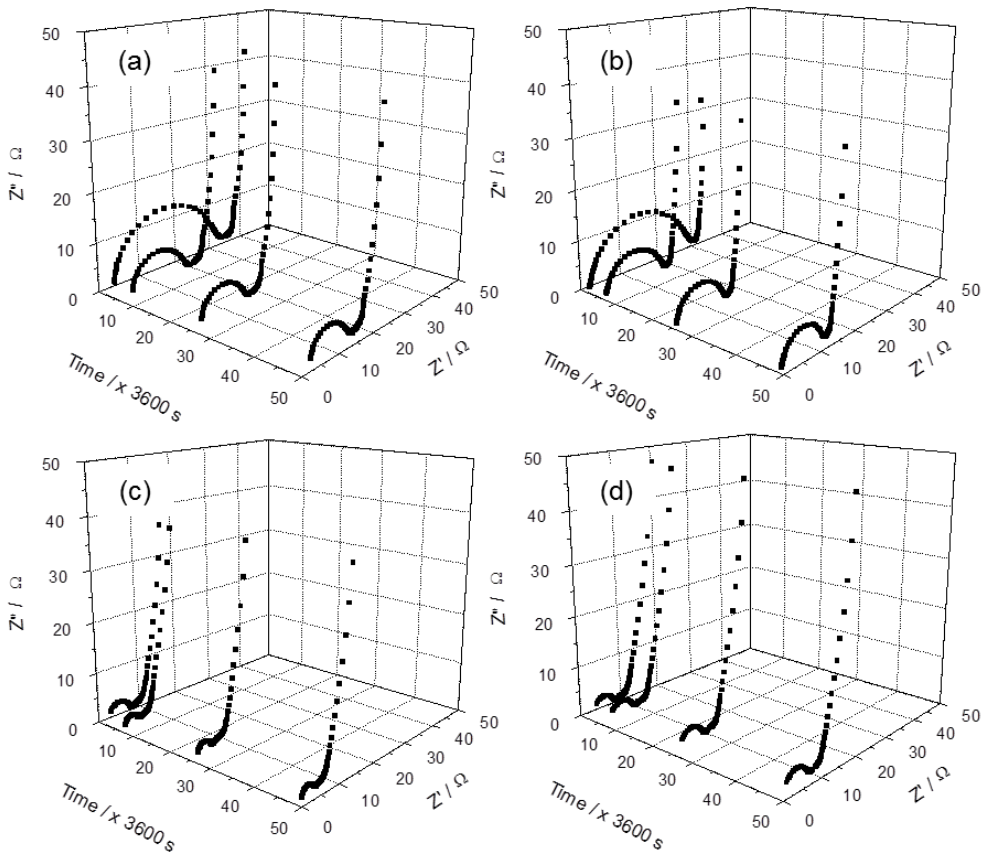

Fig. 3 Evolution of Nyquist plots with time for EDLC full cells cured at (a) 125°C, (b) 150°C, (c) 175°C and (d) 200°C.

As can be observed in Fig. 3, R_i ranges between 2 and 5 Ω among all samples and does not vary greatly with time. As described previously, R_i is associated with electrolyte resistance and, since all measurements were taken at room temperature, electrolyte conductivity is assumed to remain unaltered. Thus, the minimal increase in R_i in the cured samples is assumed to be linked to accumulation of different fractions of otherwise mobile electrolyte ions in closed pores of silica network resulting in reduced number of free conducting ions. Another possible explanation for the small variations of R_i is the variation of electrical contact resistance of the external circuit including the wire connections and coin cell holder from one system to another.

The main difference in the electrochemical behaviour of the four cells originates from the mid-range frequency region. At time 0, a charge transfer resistance of ~30 Ω was obtained for samples cured at 125 and 150 °C (Fig. 3a and b) while this value

dropped to 5 Ω as the curing temperature was raised to 175 and 200 °C (Fig. 3c and d). As mentioned previously, R_{ct} has been associated with a number of ionic and electrical components inside an EDLC. Here, the reduced R_{ct} of cells as a function of curing temperature (at time 0) can partially be attributed to the interlocking/merging effect at the electrode-electrolyte interface (see Fig. 2c and d). At higher temperatures, a layer of the gel electrolyte immobilises itself onto the electrode resulting in larger interface area between electrode and electrolyte and reducing the ionic interface resistance. Fig. 4b and c demonstrate schematics of the ionogel and porous electrode being fused together after the heating process based on the SEM images shown in section 3.2.

Furthermore, changes in R_{ct} were considerably larger for samples with 125 and 150 °C curing temperatures over the 48 h test period. The values of R_{ct} almost halved within the first 5 h of the test and continued to drop to ~30% (of R_{ct} at time 0) in both of these samples after 48 h whilst these variations were negligible for samples with the two higher curing temperatures. As mentioned in section 3.1, the physiochemical properties of [Emim][TfO] are highly dependent on temperature and a higher *k* value is achieved when curing temperature is increased. Thus, one can relate the stability of R_{ct} in samples with 175 and 200 °C curing temperatures to the maximum wetting of the AC electrode pores in these samples. A 'maximum wetted state' of activated carbon electrodes by IL takes 48 h to be achieved in samples with the two lowest curing temperatures, as the capillary forces continuously and slowly attract more IL into the AC electrode until an equilibrium state is reached. Therefore, in the investigated systems described, R_{ct} is postulated to comprise of the ionic impedance components at: (i) the electrode-electrolyte interface [25] and (ii) within the textural pores (i.e. inter-particle pores) of the AC electrodes [27,29].

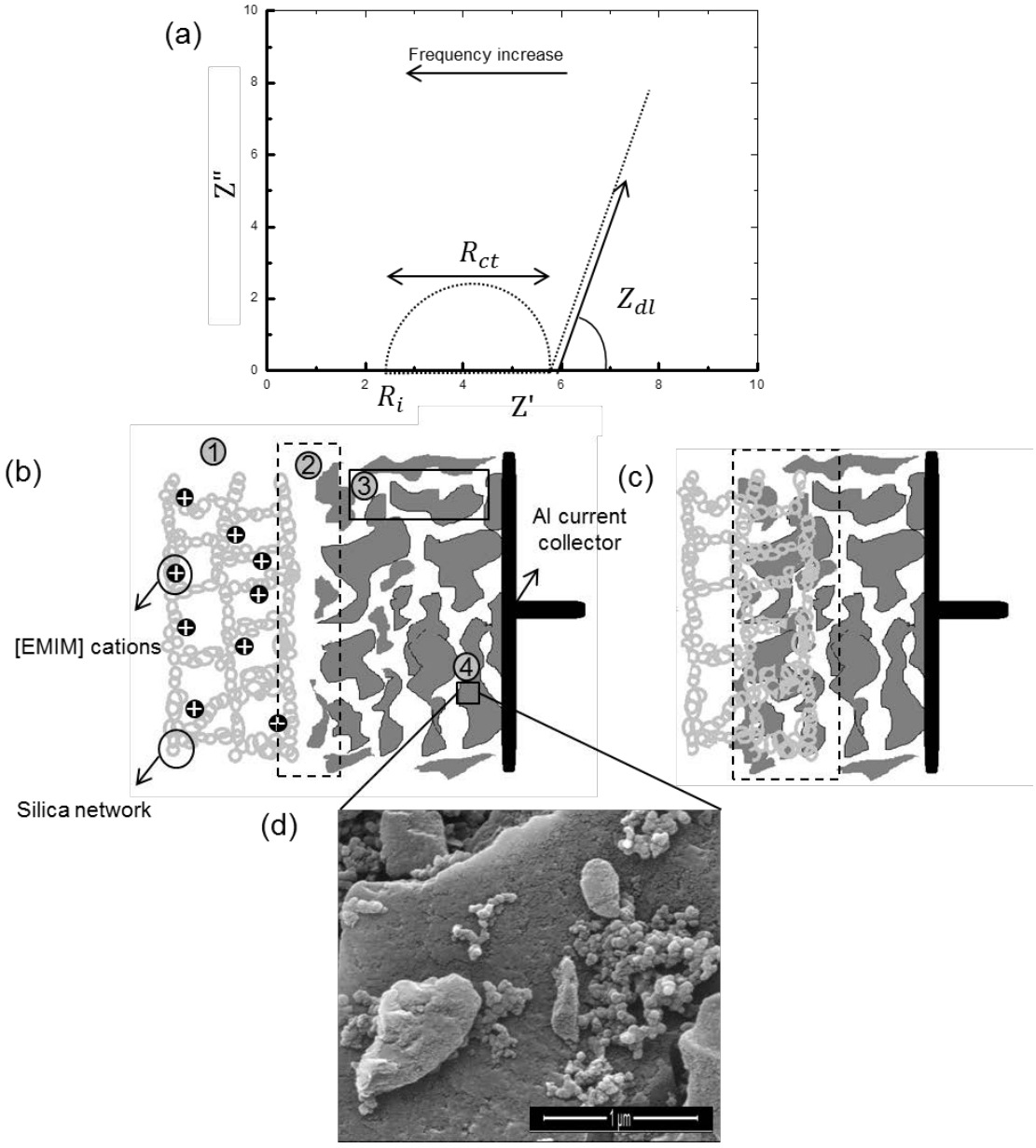

Fig. 4(a) The three main impedance components (R_i, R_{ct} and Z_{dl}) in a typical Nyquist plot for an EDLC with porous electrodes (as explained in [33]), (b) a schematic illustration of the four processes taking place during an EIS scan: 1) free movement of ions within the bulk electrolyte, 2) ion insertion into the porous electrode, 3) diffusion of ions within the textural pores of the electrode, 4) diffusion into the intra-particle pores, (c) an illustration of inter-locking effect caused by curing process and (d) an SEM image demonstrating the intra-particle pores (mesopores) in the activated carbon electrode.

To eliminate any influence from the silica network at the interface (including the possibility of onset gelation), we investigated the behaviour of an EDLC consisting of [Emim][TfO] electrolyte with equivalent volume to that inside ionogels, sandwiched between two activated carbon electrodes (with the same specifications) and

separated by a thin Celgard Inc. separator film. EIS measurements were recorded periodically in the same manner as described in section 2.4. The resultant Nyquist plots are displayed in Fig. 5. As can be seen, the diameter of the semi-circle drops (by ~31%) over the 48 h duration of the experiment, this is similar to the behaviour of ionogel-based cells. Based on room temperature experimental condition, the ionic conductivity and the physiochemical properties of the electrolyte can be presumed constant throughout the EIS experiment. Thus, these results confirm that the R_{ct} variations over time are assigned to the continuous increase in electrode wetted area by the electrolyte at the interface and the depth of the activated carbon. The stabilised R_{ct} after 48 h of the experiment indicates a maximum wetting of the electrode pores.

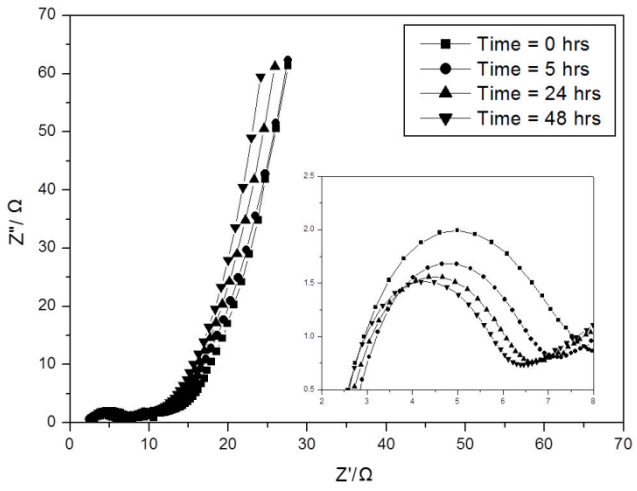

Fig. 5 Evolution of charge transfer resistance with time for EDLC full cells containing liquid [Emim][TfO] electrolyte.

As illustrated in Fig. 3, the inclining angle of all Nyquist plots is between 45° and 90° which indicates good ion diffusion into the intra-particle pores of the activated carbon electrode in all samples [34]. The slight reduction in the inclining angle for samples cured at 175 and 200 °C is ascribed to the melting and resolidifing of the PVdF binder. It is possible that during the re-solidification of the binder, some AC electrode mesopores have been blocked or narrowed and resulted in higher intra-particle ionic resistance and thus a slightly reduced inclination angle. Fig. 4b illustrates the four key ionic impedances that are present in the investigated systems. The SEM image

shown in Fig. 4d represents the intra-particle pores available in the activated carbon electrodes.

To complement the electrochemical measurements, cyclic voltammetry was used to elucidate the charge storage characteristic of the EDLC cells. The CV results at time 0 and at 48 h are shown in Fig. 6a and b respectively, together with plots of areal capacitance and R_{ct} variations as a function of time (Fig. 6c and d). The specific areal capacitances were calculated from the enclosed area in a single CV cycle using the following equations [35,36] :

$$C_T = \frac{\int I \, \mathrm{d}V}{2\Delta V S \upsilon} \tag{3}$$

$$C_{sp} = 4 \times C_T \tag{4}$$

where C_T and C_{sp} are the total specific areal capacitance and specific areal capacitance of a single electrode, respectively in mF cm^{-2}, ∫IdV is the integral of the CV curve, ΔV is the potential window, S is the total surface area of the electrode disks in cm^{-2} and υ is the scan rate.

During a voltammetry cycle, a cell is charged and discharged within a fixed potential window at a pre-set scan rate and the current response of the cell is collected. A quasi-rectangular shaped CV curve indicates fast charge propagation in the electrode and good capacitive behaviour [18,37]. On the other hand, an elliptical CV curve reflects poor current response and high internal resistance of an EDLC cell. Based on the CV plots displayed in Fig. 6a and b, all the cells showed ideal capacitive behaviour except for the case of 125 and 150 °C cured cells at time 0. Nevertheless, both cells showed quasi-rectangular CV curves after 48 h. The areal capacitances of these two cells increased by almost 60% after 48 h while this parameter increased by only 14% for the sample with 175 °C curing temperature. The capacitance remained almost unaltered throughout the 48 h period in the cell with 200 °C curing temperature. An opposite trend can be seen in the variation of R_{ct} with time (Fig. 6d) which confirms that R_{ct} is the rate limiting parameter in the electrochemical kinetics of the EDLC cells. Among all four stages of ion transport mentioned earlier, charge transfer at the electrode-electrolyte interface showed to have the most influence on the capacitive response of the EDLCs. To best our knowledge, the rate limiting effect of R_{ct} has not been shown before using electrochemical tests at room temperature (without changing the reaction rate).

Rodrigues et al. [17] concluded that ion bridging at the electrode-electrolyte interface has the highest activation energy compared to ion diffusion within the electrolyte and the electrode. Furthermore, Zheng et al. [16] showed that R_{ct} is strongly temperature dependent by performing EIS measurements at different operating temperatures. However, these studies failed to show any performance improvement of ionic liquid-based systems at room temperature. In addition, due to safety concerns with electrolyte leakage, the application of ionogels is preferred over ionic liquids. Based on the results reported here, the R_{ct} can be reduced by encapsulating ionic liquid inside a gel network and using high curing temperatures to solidify the ionogel electrolyte. This method not only reduces the electrode wetting time (i.e. higher *k* value) but also expands electrode-electrolyte interface area via a heat-induced interlocking effect. This knowledge can be useful in enhancing the system output at room temperature which is one of the major challenges with ionic liquid-based energy storage devices.

As it is shown in Fig. 6c, the areal capacitance drops in the following order: 175 °C > 150 °C > 200 °C > 125 °C -treated sample ranging from ~75 to 95 mF cm^{-2}(corresponding to 300–380 mF cm^{-2} on a single AC electrode) after 48 h. Even though R_{ct} is shown to be responsible for the variations of capacitance over the 48 h test period, the final capacitance values are influenced by the total internal resistance of each cell which includes R_i and Z_{dl} as well as R_{ct}. This is clearly seen in the case of the cells cured at 125 and 150 °C where their R_{ct} values are comparable but their capacitances are noticeably different. Previously, Brachet et al. reported a capacitance of 39 mF cm^{-2} (at 2 mV s^{-1}) at room temperature for an EDLC containing TMOS-based ionogel encapsulating 1-ethyl-3-methylimidazolium bis(trifluoromethanesulfonylimide) ionic liquid sandwiched between two activated carbon electrodes. This ionic liquid has a comparable ionic structure to that of [Emim][TfO] [10].

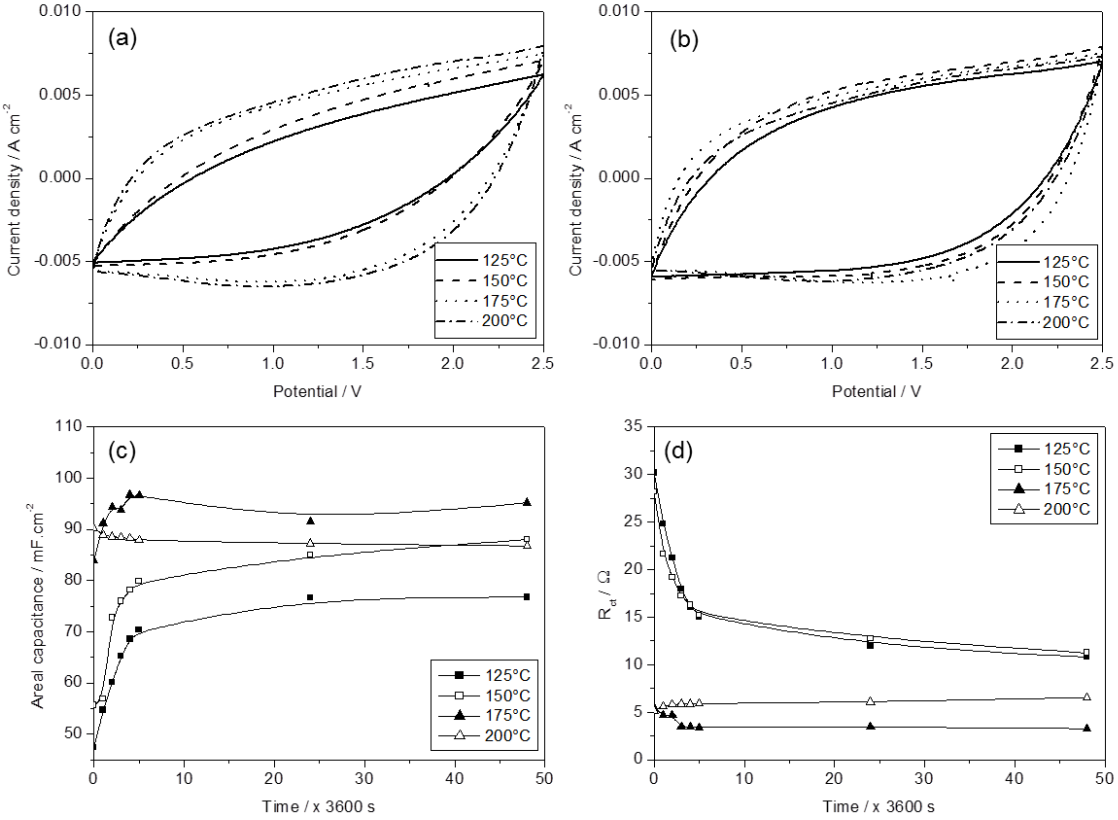

Fig. 6 Cyclic voltammetry curves of EDLCs with ionogels cured at different temperatures after (a) 0 hours and (b) 48 hours of being assembled and the variation plots of (c) areal capacitance and (d) R_{ct} as a function of time.

3.4 Visualisation of wettability using Raman line-mapping

The ionic liquid properties summarized in Table 1 and the electrochemical characterisation results suggest that the 'maximum wetted state' of the porous electrodes is achieved more quickly when ionogels are cured at higher temperatures. By reducing viscosity and improving the penetrability coefficient (*k*), ionic liquid is able to travel further through the electrode under the influence of capillary forces and wet larger volume of the active material, consequently reducing the wetting time of the porous electrode. In order to visually characterise the ingress of IL through the depth of ionogel-coated AC electrodes, Raman line-maps of the cross section of electrodes cured at 125 and 200 °C were collected. Raman microspectrometry is a powerful technique that combines the spatial resolution of an optical microscope with spectroscopic analysis to obtain molecular information from micro-scaled space within a substance. Fig. 7a illustrates the direction in which the Raman line-map was

acquired across the electrode cross section and, as it is shown, the coated electrodes were sandwiched between two thin silicon wafers to mark the start and end points of the measurements (labelled as S and E respectively) and to ensure that the electrode was positioned perpendicularly to the microscope lens. Raman spectroscopy provides information about the vibrational frequencies of covalent bonds within a sample, which can be used to determine its composition. Each material has its own unique characteristic spectrum which is sensitive to structure, orientation and its environment. However, the technique does not facilitate separation, so if there is more than one component/material within the sampled region, ~8 μm in this study, then the spectrum produced will show features for all components, leading to ambiguity of signal and making the determination of the distribution of each material at each sampling point challenging. One of the strategies that can be applied to extract discrete information from mixed signals is multivariate curve resolution (MCR), which uses algorithms such as alternating least squares (ALS) to decompose mixed spectroscopic matrices into pure component (factors) and pure concentration (loadings) matrices. The concentration of each of the pure components can then easily be determined [38–40]. In this work, four factors were utilised to account for each individual compound, namely the silicon wafer, the Al foil, activated carbon and the ionic liquid. Fig. 7b shows a direct comparison of a typical Raman spectrum of each of the pure materials present (ionic liquid, activated carbon, silicon and Al) together with the MCR calculated pure-spectral factors. As can be seen, the spectra of the pure compounds and their corresponding factors overlay very well indicating reliable MCR-output. The unexpected spikes (for e.g. in factor 4) are due to a phenomenon called Rank Deficiency caused by a combination of instrumental noise and overlap of concentration profiles of different components in the system and can reasonably be ignored [39].

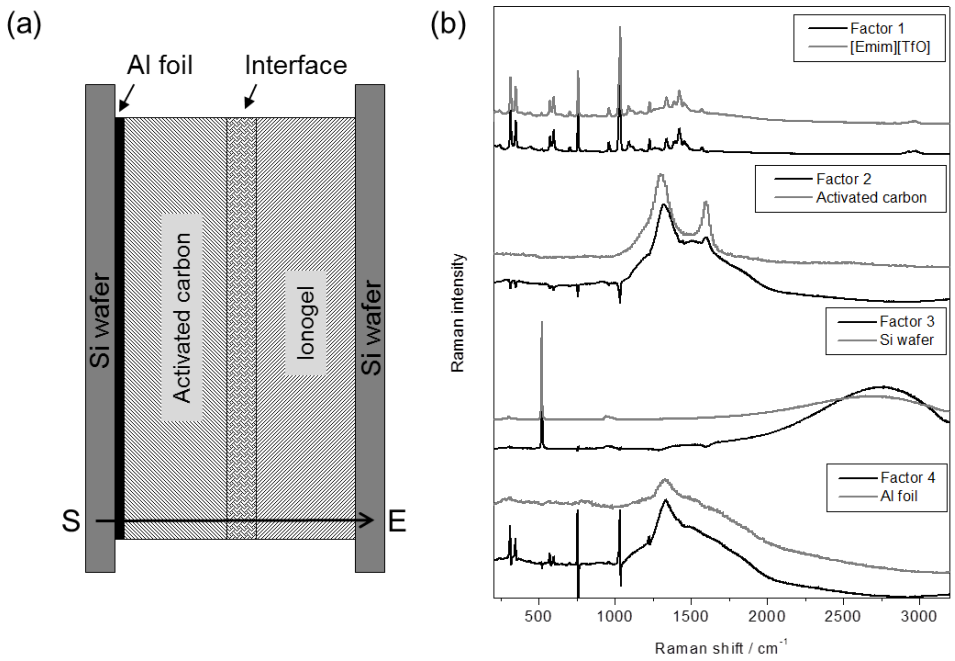

Fig. 7(a) An illustration of the line-map direction over the cross section of coated electrodes and (b) Raman spectra of the four components available in the line-map together with the corresponding MCR-recognised factors based on their variation across the cross section.

By plotting the score (or intensity at each point) of each pure component, a quantitative variation of each material across the cross section was realised as a function of location/distance travelled. Fig. 8a and b show the optical images of the electrodes that have been subjected to curing temperatures of 125 and 200 °C respectively, with the region from where the Raman data was collected being marked with dotted white lines. The corresponding Raman intensity variations of the IL from the cross sections are given in Fig. 8c and d.

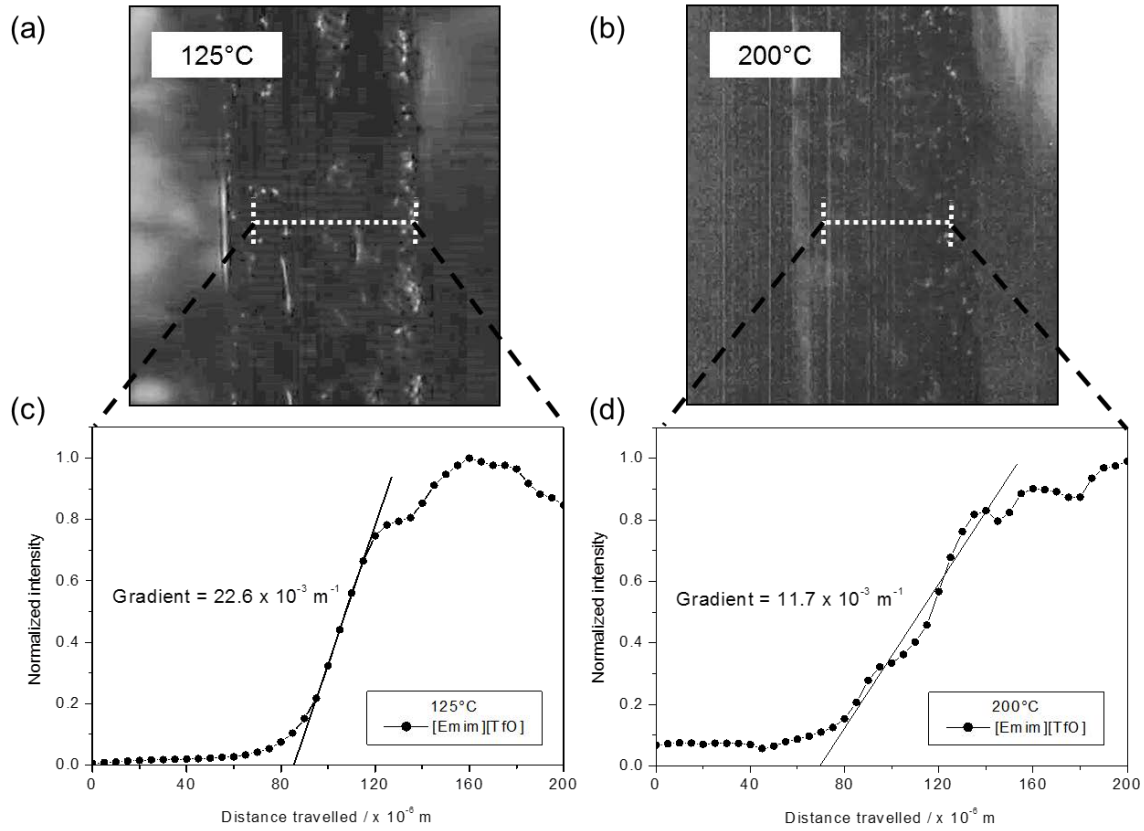

Fig. 8 (a & b) Optical images of electrodes cross section cured at 125 and 200°C and (c and d) the corresponding Raman intensity variations of [Emim][TfO] across the cross sections. The straight lines represent the best linear fits for IL distribution at the electrode-electrolyte interfaces.

Working from the left hand side of Fig. 8c relating to the sample which had been treated at 125 °C, the intensity of the IL factor, and therefore its concentration, has a low/zero intensity through the AC electrode until the interface with the IL region is reached (~70 μm). Through the interface the intensity of the IL factor increases in a quasi-linear fashion and the gradient of this line, provides information about the sharpness of the interface and by inference indicates how far [Emim][TfO] has permeated through the AC electrode pores. The analogous data for the sample which had been treated at 200 °C (Fig. 8d), shows a much broader interface with a shallower gradient and indicates that [Emim][TfO] has permeated a greater distance into the porous AC electrode. This supports the measured *k* values reported in Table 1, the high resolution SEM images (Fig. 2) and the impedance measurement results discussed in section 3.3. It is noteworthy to mention that these measurements were taken within 24 h of synthesis and represent the very early wetting stage of the electrodes by the IL. Based on the EIS results, a 'maximum wetted state' may be achieved for the sample cured at 125 °C if it was aged for an additional 24 h.

4. Conclusion

One of the great challenges with using silica-based ionogels as a scalable and industrially applicable solid electrolyte in supercapacitors is their long gelation time. Electrochemical systems containing ILs suffer from high viscosity and surface tension (compared to conventional electrolytes) which limit ion mobility and electrode wetting rate, resulting in poor electrochemical performance at room temperature. This work reports the influence of heat-assisted gelation of ionogels as a measure to counter both of these limitations. By using a high curing temperature, the gelation time of TMOS-MTMS-based ionogels was reduced to less than 90 min and as the curing temperature was increased from 125 to 200 °C the charge transfer resistance was considerably reduced, resulting in enhanced ion transport kinetics at room temperature which inferred that electrode-electrolyte interface area was increased as a result of the interlocking effect. Furthermore, the influence of elevated temperature on the penetrability coefficient of IL reduced the time needed to achieve a 'maximum wetted state' electrode determined by the capillary forces. Based on the results we can conclude that 175 °C is the optimal curing temperature for the studied system due to the minimal resultant shrinkage and excellent capacitive behaviour (95 mF cm^{-2}). This study provides an insight towards the design of safer energy storage systems that are not only industrially scalable, due to their short fabrication time, but can also be operated at room temperature as well as higher temperatures.

Funding sources

This research did not receive any specific grant from funding agencies in the public, commercial, or not-for-profit sectors.

Acknowledgements

The authors would like to thank Dr. Matrin Grüßer and his colleagues at DataPhysics who provided us with the surface tension measurements.

References

[1] A. Jänes, T. Thomberg, J. Eskusson, E. Lust, Fluoroethylene Carbonate and Propylene Carbonate Mixtures Based Electrolytes for Supercapacitors, ECS Trans. 58 (2014) 71–79. doi:10.1149/05827.0071ecs.

[2] C. Ramasamy, J. Palma Del Vel, M. Anderson, An activated carbon supercapacitor analysis by using a gel electrolyte of sodium salt-polyethylene oxide in an organic mixture solvent, J.

Solid State Electrochem. 18 (2014) 2217–2223. doi:10.1007/s10008-014-2466-3.

[3] H.H. Shen, C.C. Hu, Determination of the upper and lower potential limits of the activated carbon/propylene carbonate system for electrical double-layer capacitors, J. Electroanal. Chem. 779 (2016) 161–168. doi:10.1016/j.jelechem.2016.04.004.

[4] J. Li, J. Tang, J. Yuan, K. Zhang, Q. Shao, Y. Sun, L.C. Qin, Interactions between Graphene and Ionic Liquid Electrolyte in Supercapacitors, Electrochim. Acta. 197 (2016) 84–91. doi:10.1016/j.electacta.2016.03.036.

[5] S. Zhang, Z. Bo, H. Yang, J. Yang, L. Duan, J. Yan, K. Cen, Insights into the effects of solvent properties in graphene based electric double-layer capacitors with organic electrolytes, J. Power Sources. 334 (2016) 162–169. doi:https://doi.org/10.1016/j.jpowsour.2016.10.021.

[6] A. Lewandowski, M. Galinski, Practical and theoretical limits for electrochemical double-layer capacitors, J. Power Sources. 173 (2007) 822–828. doi:10.1016/J.JPOWSOUR.2007.05.062.

[7] M. Watanabe, M.L. Thomas, S. Zhang, K. Ueno, T. Yasuda, K. Dokko, Application of Ionic Liquids to Energy Storage and Conversion Materials and Devices, Chem. Rev. 117 (2017) 7190–7239. doi:10.1021/acs.chemrev.6b00504.

[8] J. Le Bideau, L. Viau, A. Vioux, Ionogels, ionic liquid based hybrid materials, Chem. Soc. Rev. 40 (2011) 907–925. doi:10.1039/C0CS00059K.

[9] A.I. Horowitz, M.J. Panzer, High-performance, mechanically compliant silica-based ionogels for electrical energy storage applications, J. Mater. Chem. 22 (2012) 16534–16539. doi:10.1039/C2JM33496H.

[10] M. Brachet, T. Brousse, J. Le Bideau, All Solid-State Symmetrical Activated Carbon Electrochemical Double Layer Capacitors Designed with Ionogel Electrolyte, ECS Electrochem. Lett. 3 (2014) A112–A115. doi:10.1149/2.0051411eel.

[11] A. Taubert, R. Löbbicke, B. Kirchner, F. Leroux, First examples of organosilica-based ionogels: synthesis and electrochemical behavior, Beilstein J. Nanotechnol. 8 (2017) 736–751. doi:10.3762/bjnano.8.77.

[12] D.S. Ashby, R.H. DeBlock, C.H. Lai, C.S. Choi, B.S. Dunn, Patternable, Solution-Processed Ionogels for Thin-Film Lithium-Ion Electrolytes, Joule. 1 (2017) 344–358. doi:10.1016/j.joule.2017.08.012.

[13] S. Vives, C. Meunier, Influence of the synthesis route on sol–gel SiO2–TiO2 (1:1) xerogels and powders, Ceram. Int. 34 (2008) 37–44. doi:https://doi.org/10.1016/j.ceramint.2006.08.001.

[14] K.T. Chou, B.I. Lee, Properties of silica gels prepared from high-acid hydrolysis of tetraethoxysilane, Ceram. Int. 19 (1993) 315–325. doi:10.1016/0272-8842(93)90044-R.

[15] C.A. Milea, C. Bogatu, The Influence of Parameters in Silica Sol-Gel Process, Bull. Transilv. Univ. Brasov Eng. Sci. 4 (2011) 59–66.

[16] H. Zheng, H. Zhang, Y. Fu, T. Abe, Z. Ogumi, Temperature effects on the electrochemical behavior of spinel LiMn(2)O(4) in quaternary ammonium-based ionic liquid electrolyte., J. Phys. Chem. B. 109 (2005) 13676–13684. doi:10.1021/jp051238i.

[17] M.-T.F. Rodrigues, X. Lin, H. Gullapalli, M.W. Grinstaff, P.M. Ajayan, Rate limiting activity of charge transfer during lithiation from ionic liquids, J. Power Sources. 330 (2016) 84–91. doi:https://doi.org/10.1016/j.jpowsour.2016.08.119.

[18] L. Negre, B. Daffos, V. Turq, P.L. Taberna, P. Simon, Ionogel-based solid-state supercapacitor operating over a wide range of temperature, Electrochim. Acta. 206 (2016) 490–495. doi:https://doi.org/10.1016/j.electacta.2016.02.013.

[19] N. Bengourna, F. Despetis, L. Bonnet, R. Courson, P. Solignac, H. Satha, N. Olivi-Tran, Textural , Structural and Electrical Characterizations of EMI MAc Silica Ionogels and Their Corresponding Aerogels, Appl. Phys. Res. 6 (2014) 16–25.

[20] M.S. Wu, T.L. Liao, Y.Y. Wang, C.C. Wan, Assessment of the wettability of porous electrodes

for lithium-ion batteries, J. Appl. Electrochem. 34 (2004) 797–805. doi:10.1023/B:JACH.0000035599.56679.15.

[21] R.S. Kühnel, S. Obeidi, M. Lübke, A. Lex-Balducci, A. Balducci, Evaluation of the wetting time of porous electrodes in electrolytic solutions containing ionic liquid, J. Appl. Electrochem. 43 (2013) 697–704. doi:10.1007/s10800-013-0558-x.

[22] G.W. Scherer, Sintering of Sol-Gel Films, J. Sol-Gel Sci. Technol. 8 (1997) 353–363. http://link.springer.com/article/10.1007/BF02436865.

[23] Z.H. Liu, P. Maréchal, R. Jérôme, Intermolecular interactions in poly(vinylidene fluoride) and ϵ-caprolactam mixtures, Polymer (Guildf). 37 (1996) 5317–5320. doi:https://doi.org/10.1016/0032-3861(96)00423-5.

[24] C. Lei, F. Markoulidis, Z. Ashitaka, C. Lekakou, Reduction of porous carbon/Al contact resistance for an electric double-layer capacitor (EDLC), Electrochim. Acta. 92 (2013) 183–187. doi:10.1016/J.ELECTACTA.2012.12.092.

[25] H.D. Yoo, J.H. Jang, J.H. Ryu, Y. Park, S.M. Oh, Impedance analysis of porous carbon electrodes to predict rate capability of electric double-layer capacitors, J. Power Sources. 267 (2014) 411–420. doi:10.1016/J.JPOWSOUR.2014.05.058.

[26] N.H. Basri, M. Deraman, M. Suleman, N.S.M. Nor, B.N.M. Dolah, M.I. Sahri, S.A. Shamsudin, Energy and power of supercapacitor using carbon electrode deposited with nanoparticles nickel oxide, Int. J. Electrochem. Sci. 11 (2016) 95–110.

[27] I. Yang, S.-G. Kim, S.H. Kwon, M.-S. Kim, J.C. Jung, Relationships between pore size and charge transfer resistance of carbon aerogels for organic electric double-layer capacitor electrodes, Electrochim. Acta. 223 (2017) 21–30. doi:10.1016/J.ELECTACTA.2016.11.177.

[28] K.H. An, W.S. Kim, Y.S. Park, J.M. Moon, D.J. Bae, S.C. Lim, Y.S. Lee, Y.H. Lee, Electrochemical properties of high-power supercapacitors using single-walled carbon nanotube electrodes, Adv. Funtional Mater. 11 (2001) 387–392. doi:10.1002/1616-3028(200110)11:5<387::AID-ADFM387>3.0.CO;2-G.

[29] I. Yang, S.-G. Kim, S.H. Kwon, J.H. Lee, M.-S. Kim, J.C. Jung, Pore size-controlled carbon aerogels for EDLC electrodes in organic electrolytes, Curr. Appl. Phys. 16 (2016) 665–672. doi:10.1016/J.CAP.2016.03.019.

[30] W.G. Pell, B.E. Conway, N. Marincic, Analysis of non-uniform charge/discharge and rate effects in porous carbon capacitors containing sub-optimal electrolyte concentrations, J. Electroanal. Chem. 491 (2000) 9–21. doi:10.1016/S0022-0728(00)00207-2.

[31] B.K. Kim, S. Sy, A. Yu, J. Zhang, Electrochemical Supercapacitors for Energy Storage and Conversion, Handb. Clean Energy Syst. (2015) 1–25. doi:10.1002/9781118991978.hces112.

[32] T. Gu, B. Wei, Fast and stable redox reactions of MnO2/CNT hybrid electrodes for dynamically stretchable pseudocapacitors, Nanoscale. 7 (2015) 11626–11632. doi:10.1039/c5nr02310f.

[33] S. Fletcher, V.J. Black, I. Kirkpatrick, A universal equivalent circuit for carbon-based supercapacitors, J. Solid State Electrochem. 18 (2014) 1377–1387. doi:10.1007/s10008-013-2328-4.

[34] E. Frackowiak, Electrode Materials with Pseudocapacitive Properties, in: Supercapacitors, Wiley-VCH Verlag GmbH & Co. KGaA, 2013: pp. 207–237. doi:10.1002/9783527646661.ch6.

[35] Q. Chen, X. Li, X. Zang, Y. Cao, Y. He, P. Li, K. Wang, J. Wei, D. Wu, H. Zhu, Effect of different gel electrolytes on graphene-based solid-state supercapacitors, RSC Adv. 4 (2014) 36253–36256. doi:10.1039/C4RA05553E.

[36] K.L. Van Aken, J.K. McDonough, S. Li, G. Feng, S.M. Chathoth, E. Mamontov, P.F. Fulvio, P.T.C. Yury, S. Dai, Y. Gogotsi, Effect of cation on diffusion coefficient of ionic liquids at onion-like carbon electrodes, J. Phys. Condens. Matter. 26 (2014) 284104–284114. http://stacks.iop.org/0953-8984/26/i=28/a=284104.

[37] M.F. El-Kady, R.B. Kaner, Scalable fabrication of high-power graphene micro-supercapacitors for flexible and on-chip energy storage, Nat. Commun. 4 (2013) 1475–1479. doi:10.1038/ncomms2446.

[38] J. Jaumot, R. Gargallo, A. de Juan, R. Tauler, A graphical user-friendly interface for MCR-ALS: a new tool for multivariate curve resolution in MATLAB, Chemom. Intell. Lab. Syst. 76 (2005) 101–110. doi:https://doi.org/10.1016/j.chemolab.2004.12.007.

[39] M. Garrido, F.X. Rius, M.S. Larrechi, Multivariate curve resolution-alternating least squares (MCR-ALS) applied to spectroscopic data from monitoring chemical reactions processes, Anal. Bioanal. Chem. 390 (2008) 2059–2066. doi:10.1007/s00216-008-1955-6.

[40] K.R. Fega, D.S. Wilcox, D. Ben-Amotz, Application of Raman Multivariate Curve Resolution to Solvation-Shell Spectroscopy, Appl. Spectrosc. 66 (2012) 282–288. http://as.osa.org/abstract.cfm?URI=as-66-3-282.